Inorganic Chemistry

Article

pubs.acs.org/IC

Valence State Driven Site Preference in the Quaternary Compound $Ca_5MgAgGe_5$: An Electron-Deficient Phase with Optimized Bonding

Siméon Ponou,*[,†] Sven Lidin,[†] Yuemei Zhang,[‡] and Gordon J. Miller*[,‡]

[†]Centre for Analysis and Synthesis, Chemistry Department, Lund University, Getingevägen 60, Box 124, SE-22100 Lund, Sweden

[‡]Department of Chemistry and Ames Laboratory, Iowa State University, 1605 Gilman Hall, Ames, Iowa 50011, United States

Supporting Information

ABSTRACT: The quaternary phase $Ca_5Mg_{0.95}Ag_{1.05(1)}Ge_5$ (**3**) was synthesized by high-temperature solid-state techniques, and its crystal structure was determined by single-crystal diffraction methods in the orthorhombic space group *Pnma* − Wyckoff sequence c^{12} with a = 23.1481(4) Å, b = 4.4736(1) Å, c = 11.0128(2) Å, V = 1140.43(4) Å^3, Z = 4. The crystal structure can be described as linear intergrowths of slabs cut from the CaGe (CrB-type) and the CaMGe (TiNiSi-type; M = Mg, Ag) structures. Hence, **3** is a *hettotype* of the hitherto missing n = 3 member of the structure series with the general formula $R_{2+n}T_2X_{2+n}$, previously described with n = 1, 2, and 4. The member with n = 3 was predicted in the space group *Cmcm* − Wyckoff sequence f^5c^2. The experimental space group *Pnma* (in the nonstandard setting *Pmcn*) corresponds to a *klassengleiche* symmetry reduction of index two of the predicted space group *Cmcm*. This transition originates from the switching of one Ge and one Ag position in the TiNiSi-related slab, a process that triggers an uncoupling of each of the five 8*f* sites in *Cmcm* into two 4*c* sites in *Pnma*. The Mg/Ag site preference was investigated using VASP calculations and revealed a remarkable example of an intermetallic compound for which the electrostatic valency principle is a critical structure-directing force. The compound is deficient by one valence electron according to the Zintl concept, but LMTO electronic structure calculations indicate electronic stabilization and overall bonding optimization in the polyanionic network. Other stability factors beyond the Zintl concept that may account for the electronic stabilization are discussed.

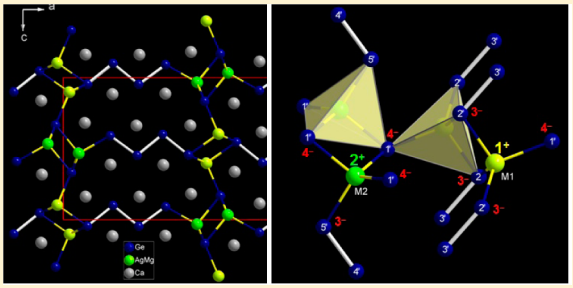

INTRODUCTION

The complex structures of some ternary and quaternary intermetallic compounds can very often be rationalized as intergrowths of relatively simple parent structures.[1−3] As such, a series of compounds can be regarded as homologues if they are built up by different combinations of two or more fragments, and this may enable the rational synthesis of other members of a given structural homology.[4] Thus, the intergrowth approach can provide the solid-state chemist with a rare heuristic concept to reliably deduce compositions, structural features, and, to some extent, properties of large families of intermetallic phases. In this context, the structure series with the general formula $R_{2+n}T_2X_{2+n}$ was rationalized by Zhao and Parthé (1989)[5] as an intergrowth of fragments cut from the TiNiSi-type and slabs of the CrB-type structures. However, only three members of this structural homology have been described yet: the $Hf_3Ni_2Si_3$-type (n = 1, space group *Cmcm*);[6] the Sc_2CoSi_2-type (n = 2, space group $C2/m$);[7] and the Sc_3NiSi_3-type (n = 4, space group $C2/m$).[8] These structures are predicted to be monoclinic $C2/m$ for n even or orthorhombic *Cmcm* when n is an odd number.[5]

The reported members of this homology involve rare-earth or early (group 4) transition metals.[9] So far, only two alkaline-earth homologues have been reported: the polymorphic Ca_2NiSn_2[10] with a Sc_2CoSi_2-type monoclinic modification; and the monoclinic $Ca_3Ag_{1.33}Ge_{2.67}$[11] with the Sc_3NiSi_3-type structure. Interestingly, both Ca compounds are formally charge-balanced Zintl phases. Hence, because of the electronic stabilization, further members of the Ca subfamily $Ca_{2+n}M_{2+x}Ge_{2-x+n}$ are expected to comply with the Zintl−Klemm concept. For instance, the n = 3 member, "$Ca_5Ag_{2+x}Ge_{5-x}$", with x = 2/3, should be charge-balanced and will represent the still missing member with n = 3. However, to our surprise, attempts to rationally prepare this phase have remained elusive. Having in mind that CaMgGe adopts the TiNiSi-type structure, an alternative compound "$Ca_5Mg_2Ge_5$" with divalent Mg can be predicted to adopt the target structure as a fully ordered and electron precise Zintl phase, but attempts to prepare the ternary Mg phase also failed. Recently, we embarked on assessing the experimental limit of the electronic flexibility of the TiNiSi-type structure. Hence, *alio*-valent partial substitutions of monovalent Ag by divalent Mg or trivalent Al in CaAgGe with a TiNiSi-type superstructure[11−13] were conducted under the hypothesis that the superstructure will be suppressed only when the valence electron (ve) count corresponds to the limit of the Zintl concept (8 ve/formula unit). Surprisingly, in the case of Mg, the reaction yielded the Ag-poor compound $CaMg_{1-x}Ag_xGe$ with the Ag content limited to x = 0.13(3).[13] Finally, the

Received: February 26, 2014
Published: April 18, 2014

   dx.doi.org/10.1021/ic500449d | *Inorg. Chem.* 2014, 53, 4724−4732

missing member of the structure series $Ca_{2+n}M_{2+x}Ge_{2-x+n}$, with $n = 3$, was serendipitously obtained during similar Ag substitution by Mg metal in the Zintl phase $Ca_3Ag_{1+x}Ge_{3-x}$ ($x = 1/3$).[11] In this Article, the synthesis and the crystal structure of this new quasi-ternary phase $Ca_5Mg_{0.95}Ag_{1.095(1)}Ge_5$ (**3**) are reported. It crystallizes in the unexpected space group *Pnma* and is one-electron-deficient according to the Zintl concept.[14] The rationale for the symmetry reduction from the predicted space group *Cmcm*, as well as the site preference between Mg and Ag, is provided. Also, other factors beyond the Zintl concept, which may account for the overall electronic stabilization of **3**, are investigated with the help of the LMTO band structure calculations.

EXPERIMENTAL SECTION

Synthesis and Analysis. The starting materials for the synthesis were the elements, Ca (granule, 99.5%), Ge (50 μ powder, 99.999%), Ag (60 μ powder, 99.9%), and Al (Ingot, 99.999%) all from ABCR (Karlsruhe, Germany), which were stored in an argon-filled glovebox and used as received. The mixture (ca. 600−700 mg) with the atomic ratio Ca:Mg:Ag:Ge = 3:1:1:2 was arc-sealed in Nb/Ta tubes under an Ar atmosphere. This stoichiometry was chosen because $Ca_3Ag_{1+x}Ge_{3-x}$ ($x = 1/3$) was obtained similarly from Ca:Ag:Ge = 3:2:2. The sealed Nb ampules were then enclosed in a fused silica glass Schlenk tube under vacuum (ca. 10^{-2} mbar). The reactions were carried out inside a programmable tubular furnace by heating from room temperature up to 980 °C in 10 h. After 1 h, the furnace was cooled down to 870 °C at 2 °C/min, and the sample was annealed for at least 5 days. Finally, the oven was switched off to allow the product to cool down to room temperature. Routine analysis by powder X-ray diffraction on a Stoe diffractometer (Ge(111) monochromator for Cu−Kα_1 radiation: λ = 1.54056 Å) equipped with a linear position sensitive (PSD) detector indicated that the resulting air- and moisture-sensitive products are multiphasic with a larger amount of the title compound in the form of highly reflective black crystals with bulky shapes and some undesired phases, including $CaMg_{1-x}Ag_xGe$ (TiNiSi-type, $x = 0.13$)[13] and other unidentified phases, that are generally in the form of microcrystalline powder (no single crystal of these side products was found in the sample). In addition, single crystals from the reaction of the mixture Ca:Mg:Ag:Ge = 6:1:2:4, with a lower amount of Mg, were refined, yielding the composition $Ca_5Mg_{0.88}Ag_{1.12(1)}Ge_5$. Unfortunately, the refinement of single-crystal X-ray diffraction data from this sample was not satisfactory (R_1 = 18% for all reflections) due to poor quality of the single crystals. Hence, the phase width could not be assessed precisely. Also, the synthesis of the end member, i.e., Ag-free phase, remains elusive.The chemical composition of crystals of the title compound were verified with an SEM using a field emission scanning electron microscope (JSM-7000F, JEOL, Japan) operating at 15 kV and equipped with an energy-dispersive X-ray spectrometer EDX system (INCAx-sight, Oxford Instruments, U.K.). The analysis on several single crystals of the title phase confirmed the presence of all four elements with the atomic ratio (in percentage) Ca:Mg:Ag:Ge = 41(1):07(1):09(1):43(1), which is close to the refined value Ca:Mg:Ag:Ge = 41.7:07.9:08.7:41.7.

Single-Crystal X-ray Data Collection and Structural Refinement. Crystal data, data collection, and structure refinement details are summarized in Table 1, and Table 2 contains the atomic positions and equivalent displacement parameters. Because of their air-sensitive character, the crystals were mounted on a glass fiber and sealed in a glass capillary inside an argon-filled glovebox. Single-crystal X-ray diffraction data collection was completed at ambient temperature on an Oxford Diffraction Xcalibur3 diffractometer with a CCD detector (Oxford Diffraction Ltd., U.K.), using graphite monochromatized Mo−Kα radiation (λ = 0.71073 Å), operated at 50 kV and 40 mA, and a detector-to-crystal distance of 50 mm. A full set of data were obtained in the ω-scan mode with a 0.75° rotation width and a 5 s exposure time per frame. Absorption correction based on a semiempirical "multiscan" approach was applied to the integrated reflections using the program CrysAlis RED.[15] The structure was solved by using direct methods, and full-matrix least-squares refinement on F^2 was carried out using the SHELXTL program package.[16,17] In the TiNiSi-related slab, it was not possible to assign all atomic sites based on electron density only. This is because some Ag/Mg mixed sites may have comparable electron density as Ge atoms. Hence, our starting model, which turned out to be inaccurate, was based on a previous prediction,[5] and also by analogy to the $n = 4$ homologue, which features Ge_2 dumbbells in the TiNiSi-related slabs and Ag atoms at the interface of the two structural blocks.[11] Then, we

Table 1. Crystallographic Data and Refinement Parameters for $Ca_5M_2Ge_5$ (M = Ag/Mg)

empirical formula	$Ca_5Mg_{0.95}Ag_{1.05(1)}Ge_5$ (**3**)
formula weight	699.71
crystal color and habit	reflective black regulus
crystal size	0.08 × 0.05 × 0.04 mm^3
temperature	293(2) K
crystal system/space group	orthorhombic/*Pnma* (No. 62)
unit cell parameters (Å)	a = 23.1481(4)
	b = 4.4736(1)
	c = 11.0128(2)
unit cell volume/Z	1140.43(4) Å^3/4
density calculated	4.075 g/cm^3
abs. coeff. (Mo Kα)	17.01 mm^{-1} (λ = 0.71073 Å)
index range	$-33 \le h \le 32$, $-6 \le k \le 6$, $-9 \le l \le 16$
θ range	3.7−32.2°
reflns collected	10577 (R_σ = 0.045)
independent reflns	2138 (R_{int} = 0.045)
data completeness	95.3%
F(000)	1283
absorption correction	empirical
refinement method	full-matrix least-squares on F^2(SHELXL97)
parameters	77
goodness-of-fit on F^2	1.091
observed reflns [$I > 2\sigma(I)$]	1594
final R indices [$I > 2\sigma(I)$]	R_1 = 0.0368, wR_2 = 0.0701
final R indices (all data)	R_1 = 0.0586, wR_2 = 0.0734
extinction coefficient	0.0026(1)
residual map (e$^-$/Å^3)	1.708/−1.064
ICSD-number[a]	426 855

[a]Further details of the crystal structure investigations may be obtained from the Fachinformationszentrum Karlsruhe, 76344 Eggenstein-Leopoldshafen, Germany (Fax: +49 7247 808 666; E-Mail: crysdata@fiz-karlsruhe.de).

Table 2. Wyckoff Sites, Atomic Coordinates, and Equivalent Isotropic Displacement Parameters (Å^2) for $Ca_5Mg_{0.95}Ag_{1.05(1)}Ge_5$ (3)

atom	Wyckoff	x	y	z	U_{eq} (Å^2)
Ge1	4*c*	0.97356(3)	1/4	0.3324(1)	0.0095(2)
Ge2	4*c*	0.91944(3)	1/4	0.9547(1)	0.0100(2)
Ge3	4*c*	0.83319(3)	1/4	0.0997(1)	0.0099(2)
Ge4	4*c*	0.74713(3)	1/4	0.9525(1)	0.0095(2)
Ge5	4*c*	0.65717(3)	1/4	0.0909(1)	0.0095(2)
M1[a]	4*c*	0.02027(3)	1/4	0.1026(1)	0.0144(2)
M2[b]	4*c*	0.55167(6)	1/4	0.9668(1)	0.0142(4)
Ca1	4*c*	0.07417(6)	1/4	0.8373(1)	0.0135(3)
Ca2	4*c*	0.92774(6)	1/4	0.6813(1)	0.0130(3)
Ca3	4*c*	0.16470(6)	1/4	0.1154(1)	0.0105(3)
Ca4	4*c*	0.34180(6)	1/4	0.1127(1)	0.0113(3)
Ca5	4*c*	0.25477(6)	1/4	0.8380(1)	0.0113(3)

[a]M1: 0.782(3) Ag + 0.218(3) Mg. [b]M2: 0.733(3) Mg + 0.267(3) Ag.

dx.doi.org/10.1021/ic500449d | Inorg. Chem. 2014, 53, 4724−4732

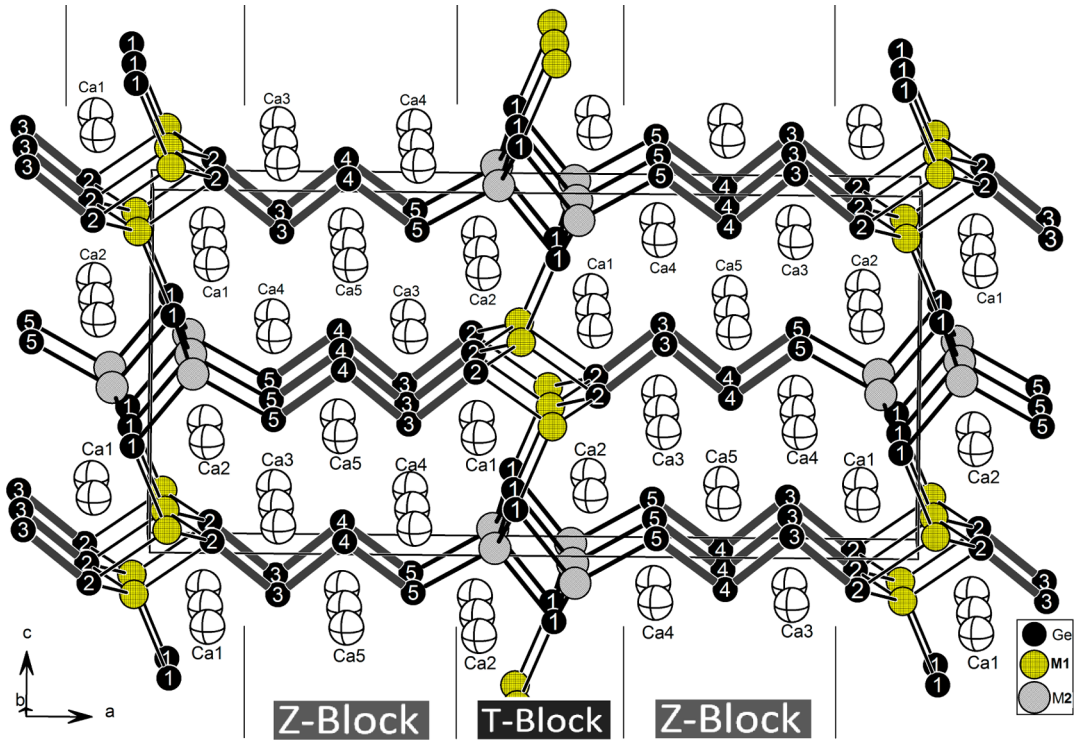

Figure 1. Projection of the structure of $Ca_5(Mg/Ag)_2Ge_5$ in the *b*-direction, emphasizing the intergrowth of TiNiSi- and CrB-type related slabs, referred to as T- and Z-blocks, respectively. The atoms are labeled according to Table 2

assumed that Mg will mix only at Ag positions similar to Al behavior in the corresponding solid solution of the $n = 4$ member. This structure model shows some unfavorably short Mg−Ag distances of 2.711 Å due to Ag mixing at one Ge site, and a short M−Ge distance of 2.556 Å, which is more consistent with a Ge−Ge bond distance. In this model, the Ge atoms are also in two different coordination geometries, including a tetrahedral geometry (albeit very distorted), a result that is not consistent with the expected negative oxidation state of Ge. The starting model was, therefore, corrected, based on interatomic distances and coordination geometry, by assigning only Ge to the more trigonal-pyramidal and Mg/Ag to the more tetrahedral positions. The refinement of the final model converged to $Ca_5Mg_{0.95}Ag_{1.05(1)}Ge_5$, in good agreement with the nominal composition of the starting mixture. The images were rendered using the program Diamond, version 2.1c.[18]

Electronic Structure Calculations. The electronic structures and chemical bonding were investigated on the basis of the density functional theory (DFT) using the tight-binding linear muffin-tin orbital (TB-LMTO-ASA) approach and the local-density approximation (LDA)[19] within the program LMTO47c.[20] Since the crystal structure of $Ca_5Mg_{0.95}Ag_{1.05(1)}Ge_5$ exhibits mixed occupied sites, ordered models were used for calculations. In the model 1, the M1 sites are fully occupied with Ag (exp.: 0.78 Ag + 0.22 Mg), whereas the M2 sites are fully occupied with Mg (exp.: 0.73 Mg + 0.27 Ag). In addition, the Mg-only imaginary phase "$Ca_5Mg_2Ge_5$" (with Mg at both the M1 and M2 sites) was considered in order to verify further the electron requirement. The radii of the muffin-tin spheres were determined by an automatic procedure.[21] No empty spheres were needed. The *k*-space integration was performed by the tetrahedron method on a set of 325 irreducible *k*-points and a basis set with Mg-3*s*/3*p*, Ca-4*s*/(4*p*)/3*d*, Ge-4*s*/4*p*/(3*d*), and Ag-5*s*/5*p*/4*d* (down-folded orbitals in parentheses). The crystal orbital Hamilton population (COHP)[22] was used for analysis of the orbital interactions and relative covalency contributions to the overall bond strengths. Since the COHP is an energy partitioning, negative/positive values indicate bonding/antibonding interactions. The Fermi level in all figures is taken as the zero energy level, and the COHP curves are drawn by reversing their values with respect to the energy scale (i.e., −COHP vs *E*). Hence, the calculated peak values become negative for antibonding and positive for bonding interactions.Furthermore, to understand the site preference, total energy calculations were performed on model 1 defined above and an additional model 2 with Ag at M2 site and Mg at M1 site, by using the projector augmented wave method (PAW) of Blöchl[23] coded in the Vienna *Ab-initio* Simulation Package (VASP).[24] We employed the generalized gradient approximation (GGA) with exchange and correlation treated by Perdew−Burke−Enzerhoff (PBE),[25] with a 2 × 12 × 4 *k*-points grid. The cutoff energies for the plane-wave expansions were 400 eV. For the PAWs, we considered 17 valence electrons for Ag ($4p^64d^{10}5s^1$), 8 for Mg ($2p^63s^23p^0$) and Ca ($3p^64s^24p^03d^0$), and 4 for Ge ($4s^24p^2$). The self-consistent criterion for the energy was 0.001 meV. Finally, the structure was optimized with respect to lattice parameters and internal degrees of freedom.

RESULTS AND DISCUSSION

The compound $Ca_5Mg_{0.95}Ag_{1.05(1)}Ge_5$ (**3**) crystallizes in the orthorhombic space group *Pnma* (Pearson *oP*48) and represents a new member of the structure series $Ca_{2+n}M_{2+x}Ge_{2+n-x}$ (M = Ag, Mg, Al), with $n = 3$ and $x = 0$. This corresponds to the Ca subfamily of the larger structure series $R_{2+n}T_2E_{2+n}$ (E = Si, Ge) that has been described for $n = 1$, 2, and 4 for a wide range of rare-earth metals (R) and with essentially Fe, Co, and Ni as transition metals (T).[26,27] Therefore, the structure of **3** is best described using the chemical twinning approach as the result of a topological fusion of fragments of CaMGe (TiNiSi-type with M = Mg/Ag)[11,28,29] and CaGe (CrB-type)[30] structures. The member with $n = 3$ was predicted to adopt the space group *Cmcm*,[5] with only seven atomic positions, Wyckoff sequence f^2c^2. Thus, in the experimental space group, *Pnma*, the five 8*f* sites become split, each into two 4*c* sites. According to the *Bärninghausen* formalism, *Pnma* in its nonstandard setting, *Pmcn*, corresponds to a *klassengleiche* maximal subgroup of index two (k_2) of the space group *Cmcm*, with an origin shift of $(-^1/_4\ -^1/_4\ 0)$.[31,32]

dx.doi.org/10.1021/ic500449d | *Inorg. Chem.* 2014, 53, 4724−4732

A view of the $Ca_5MgAgGe_5$ structure emphasizing its intergrowth structure is provided in Figure 1, and selected bond distances are listed in Table 3. The predicted model was

Table 3. Selected Bond Lengths for $Ca_5Mg_{0.95}Ag_{1.05(1)}Ge_5$ (3)

atom pair (× n)[a]		distance/Å	atom pair (× n)[a]		distance/Å
Ge1	−M2 (× 2)	2.745(1)	Ca1	−Ge1 (× 2)	3.117(1)
	−M1 (× 1)	2.752(1)		−Ge3 (× 2)	3.176(1)
	−M2 (× 1)	2.857(1)		−M1 (× 1)	3.177(2)
Ge2	−Ge3 (× 1)	2.557(1)		−M1 (× 2)	3.197(1)
	−M1 (× 2)	2.711(1)		−Ge2 (× 2)	3.206(1)
Ge2	−M1	2.846(1)	Ca2	−Ge5 (× 2)	3.140(1)
Ge3	−Ge4	2.569(1)		−Ge1 (× 2)	3.201(1)
Ge4	−Ge5	2.581(1)		−M2 (× 2)	3.289(1)
Ge5	−M2	2.799(1)		−M2 (× 1)	3.300(2)
				−M1 (× 1)	3.481(1)
Ca3	−Ge2 (× 2)	3.065(1)	Ca4	−Ge1 (× 1)	3.110(2)
	−Ge4 (× 2)	3.119(1)		−Ge4 (× 2)	3.123(1)
	−Ge5 (× 1)	3.239(1)		−Ge5 (× 2)	3.167(1)
	−Ge3 (× 2)	3.259(1)		−Ge3 (× 1)	3.173(2)
				−M2 (× 2)	3.442(1)
Ca5	−Ge3 (× 2)	3.102(1)	Ca5	−Ge4 (× 1)	3.204(2)
	−Ge5 (× 2)	3.126(1)		−Ge4 (× 2)	3.214(1)

[a]M1: Ag1/Mg = 0.782(3)/0.218(3). M2: Mg2/Ag = 0.733(3)/0.267(3).

first assumed, and later corrected according to interatomic distances and coordination geometry, by assigning Ge to the more trigonal-pyramidal and Mg/Ag to the more tetrahedral sites. The resulting model indicates a splitting of the Ge_2 dumbbells by switching one Ge position with neighboring Ag atoms at the interface. The coloring in the final model that also avoids Ag−Mg short distances is represented in Figure 2, alongside with the n = 4 model for comparison. Mg−Ag direct contacts ranging from 2.88 to 2.95 Å are observed in some ternary phases such as $CaMg_{0.98}Ag_{1.02}$ (TiNiSi-type) where partial Ag/Mg mixing is also observed.[33] However, in this phase as well as in the fully ordered REMgAg (RE = rare-earth),[34] the Ag atoms are most likely in a negative oxidation state, according to the crystallochemical trend in the TiNiSi-type family.[35]

There are 12 unique crystallographic sites in the asymmetric unit, all at special positions (Wyckoff site 4c) on the mirror plane at $y = {}^1/_4$ (Table 2): five sites are assigned to Ca, two are Ag/Mg mixed (M) sites, and five correspond to Ge atoms. Three Ge positions are two-bonded atoms located in the CrB-related slabs (Z-block). In the TiNiSi-related slabs (T-block), the two remaining Ge sites (Ge1 and Ge2) are four-coordinated, in a rather trigonal-pyramidal geometry, but having a very different surrounding (Figure 2a). The Ge1 atoms without homonuclear contact are connected to four M sites (1M1 + 3M2), and at the interface, the Ge2 surroundings (3M1 + 1Ge3) include one connection to Ge3 of the Z-block. Likewise, the M1 and M2 positions in the T-block are tetrahedrally surrounded by Ge atoms, albeit highly distorted. The M1 and M2 mixed sites differ by their relative occupancies of Mg and Ag atoms, but have similar coordination geometries. The strong anisotropy in bond distances here is typical of the TiNiSi parent structure, and the increase of the bond distances from M1−Ge1 to M2−Ge1 is consistent with the relative occupancy of the Mg and Ag atoms in the respective atomic sites.

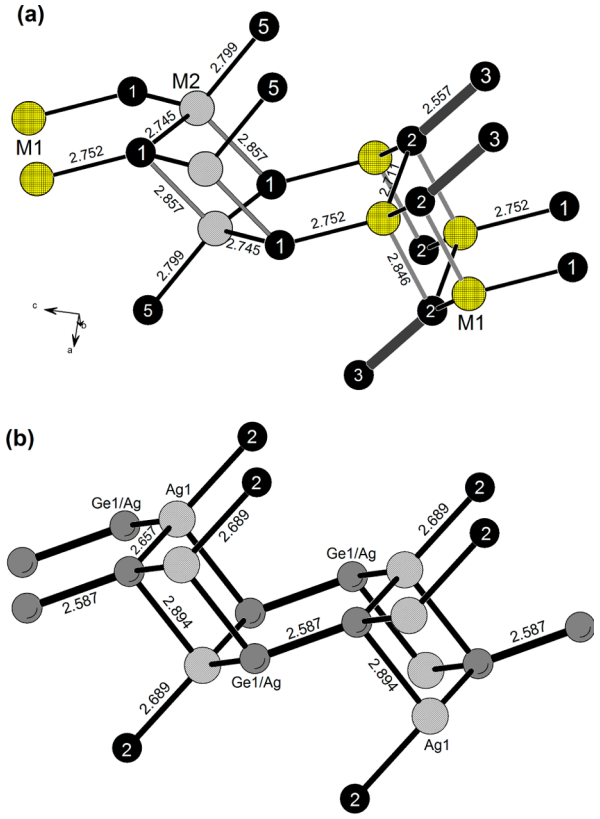

Figure 2. (a) Close view of the atomic ordering and connectivities in the TiNiSi-related slabs of the final model, and (b) the corresponding view in the n = 4 homologue with monoclinic $C2/m$ where favorable Ag···Ag (d^{10}−d^{10} like) interactions allow Ge/Ag mixing. The bond distances are indicated in Å. The black spheres are Ge atoms.

The Ge positions in the Z-block are characterized by homonuclear contacts with the Ge−Ge bond distances ranging from 2.557 to 2.581 Å, very comparable to those observed in the parent structure CaGe (2.592 Å),[30] and also to those in the n = 4 member with distances of 2.544 and 2.582 Å.[11] One terminal Ge atom of the tetramers (here Ge5) in the Z-block is further connected to the metal sites M2 (distance 2.779 Å) and the other terminal Ge2 is three connected to the M1 sites of the T-block (Ge2−M1 = 2.711 and 2.846). Hence, the most noticeable structure motifs in **3** are the four-membered Ge_4 chains with a *trans* conformation and MGe_4 tetrahedra that are condensed by sharing edges and a corner (Figure 3). In the CrB-related substructure, a trigonal prismatic coordination of the Ge atoms by Ca atoms is observed, repeating a typical feature of the parent structure CaGe (Figure 4), with the Ca−Ge distances between 3.119 and 3.259 Å. In the T-block, the Ca−Ge distances are between 3.065 and 3.206 Å.

Topologically, the polyanionic substructure of **3** is characterized by a complex ($MgAgGe_5$) three-dimensional (3D) open framework of two four-bonded and four two-bonded Ge atoms, as well as two four-connected M sites, with the cationic-like Ca atoms located in the large 14-membered channels. The 3D framework can be subdivided into two blocks with distinct structural motifs. The *first block* consists of M_2Ge_2 layers extending in the *bc*-planes and stacked along the *a*-direction at $x = 0$ and $x = {}^1/_2$ with an ···AB··· sequence (Figure 1). Alternatively, the T-block can be viewed as being composed of (M_2Ge_2) "ladders" of four-membered rings running in the *b*-direction and connected by Ge−M bonds in the *c*-direction to

dx.doi.org/10.1021/ic500449d | Inorg. Chem. 2014, 53, 4724−4732

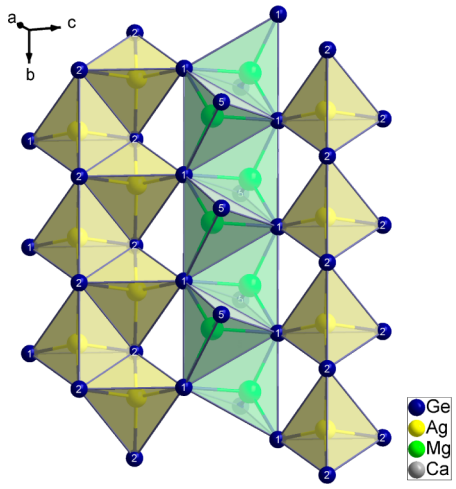

Figure 3. Polyhedral view of the Mg (M2) and Ag (M1) centered Ge_4 tetrahedra in the T-block showing their condensation by sharing edges and corners to form an infinite sheet parallel to the (100) plane.

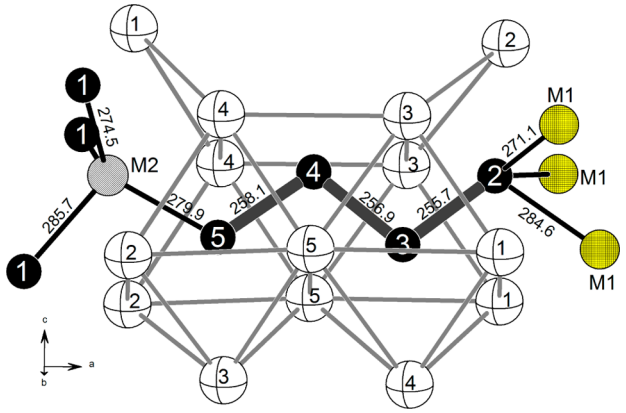

Figure 4. Local environment and connectivity of the Ge atoms in the CrB-related slabs and at the interface: Note the (reversal) similarity between Ge2 and M2. The interatomic distances are given in pm.

form 2D sheets that extend in the *bc*-plane. The obvious difference between the T-blocks in the monoclinic $n = 4$ member and the orthorhombic $n = 3$ member is the shape of the four rings that make up the ladders. The rectangular ladders in the latter are significantly tilted as compared to those in the former structure. The same difference is also observed between the parent structures KHg_2 (space group *Imma*) and its ternary derivative TiNiSi (space group *Pnma*).[35,36] Therefore, the T-block in **3** is more typical of the TiNiSi structure so that the ladders are also connected by heteronuclear Ge−M bonds. In contrast, the T-block of the $n = 4$ member is more typical of the KHg_2-type structure. The *second block* involves Ge_3 trimers in a zigzag conformation of two-bonded Ge atoms that are connected to the (M_2Ge_2) layers through M−Ge connections at one end and, at the other, by a Ge−Ge bond, resulting in the Ge_4 tetramer (Figure 4). Thus, the structure of **3** can be deduced from the predicted model by breaking up the Ge_2 dumbbells and switching the Ag position with one of the two Ge atoms forming the dumbells. As a result of this, homonuclear Ge−Ge bonds are not observed in the TiNiSi-related block, but only in the CrB-related block and at the interface of the two blocks. In contrast, in the $n = 4$ homologue, $Ca_3Ag_{1+x}Ge_{3-x}$ ($x = 1/3$), only Ag−Ge contacts are observed at the interface between the two distinctive T- and Z-blocks (Figure 3). As for the $n = 4$ homologue, the CrB-related slabs are chemically very rigid because no subsitution/mixing is observed, whereas the TiNiSi-related fragments retain the structural and electronic flexibility of the parent structure by accommodating very different types of elements, such as the *s*-block metal Mg with the transition metal Ag and *p*-block element Ge within the same anionic framework, although their atomic radii[37] are significantly different, with 1.22, 1.44, and 1.60 Å, for Ge, Ag, and Mg, respectively.

According to the Zintl concept, one can assume that the more electropositive metals Ca are involved in mainly ionic-type interactions (all Ca−X distances are longer than 3.0 Å). Hence, closed-shell, isolated $[Ge]^{4-}$ and $[Ge_4]^{10-}$ polyanions are expected, and this can be expressed in the Zintl-type formulation as $(Ca^{2+})_5(Mg^{2+})(Ag^{+})[(1b\text{-}Ge^{3-})_2(2b\text{-}Ge^{2-})_2]\text{-}[(0b\text{-}Ge^{4-})](h^{+})$, in which 1*b*-, 2*b*-, and 0*b*- denote one, two, or zero-bonded atoms, respectively; h^+ represents a missing one-electron donor. Thus, the compound is one electron deficient per formula unit. Zintl phases are electronically charge-balanced with closed-shell configurations for all atoms. Electron-deficient or electron-rich phases are interesting because they provide test cases for probing the limits of the Zintl concept.[38−40] Hence, two unusual structural features of this apparently electron-deficient phase are the Mg/Ag site preference and the Ge_4 oligomer. Other prominent phases featuring four-membered chains of highly charged Ge atoms include the electron precise $n = 4$ homologue,[11] the two-electron-deficient binary phases Ae_7Ge_6 (Ae = Ca, Sr, Ba),[41] and the one-electron-rich phase, Ca_4InGe_4.[42] An analogous tin tetramer, Sn_4, has been described in $Ca_6Cu_2Sn_7$.[43] In all of these cases, the tetrameric chains are in higher local symmetry with point group C_{2h}, but in the title compound, the Ge atoms of the tetramer (local point group C_s) are not related by symmetry. One consequence of the symmetry breaking is that, if one assumes closed-shell configurations for all Ge atoms in the tetramer, the terminal Ge atoms having the same formal charges are in markedly different chemical environments (Figure 4) with Ge2 connected to three M1 sites and Ge5 connected to only one M2 site. Intuitively, this implies that the chemical potential of the two terminal Ge atoms will be very different, and a strong gradient of chemical potential should result within the oligomeric unit. We can speculate that the electron shortage is meant to counterbalance the resulting instability. As suggested in the case of Ae_7Ge_6 phases, which are two valence electrons short according to the 8−*N* rule, the formation of partial Ge═Ge double bonds in the tetramer would result in a charge-balanced situation.[41] However, the Ge−Ge distance in α-Ge is 2.45 Å, much shorter than those observed in **3**. The longer bond distance is generally attributed to the negative charge on the Ge atom, resulting in enhanced electrostatic repulsion. Meanwhile, the remarkable site preference between Mg and Ag atoms is apparently correlated with the asymmetry of the Ge_4 tetramer and, therefore, deserves special attention. This is manifested by different compositions of the M1 and M2 mixed sites within the TiNiSi-related slabs with Ag preferring the M1 sites and Mg the M2 sites at the interface and represents an interesting case of site preference or the "coloring problem" in a solid solution.[44,45] Although significant, the difference in atomic radii (Ag 1.44 and Mg 1.60 Å) alone cannot justify the observed site preferences because both metals are in similar tetrahedral coordination by Ge atoms. In fact, the Mg/Ag coloring in the system seems to

dx.doi.org/10.1021/ic500449d | *Inorg. Chem.* 2014, 53, 4724−4732

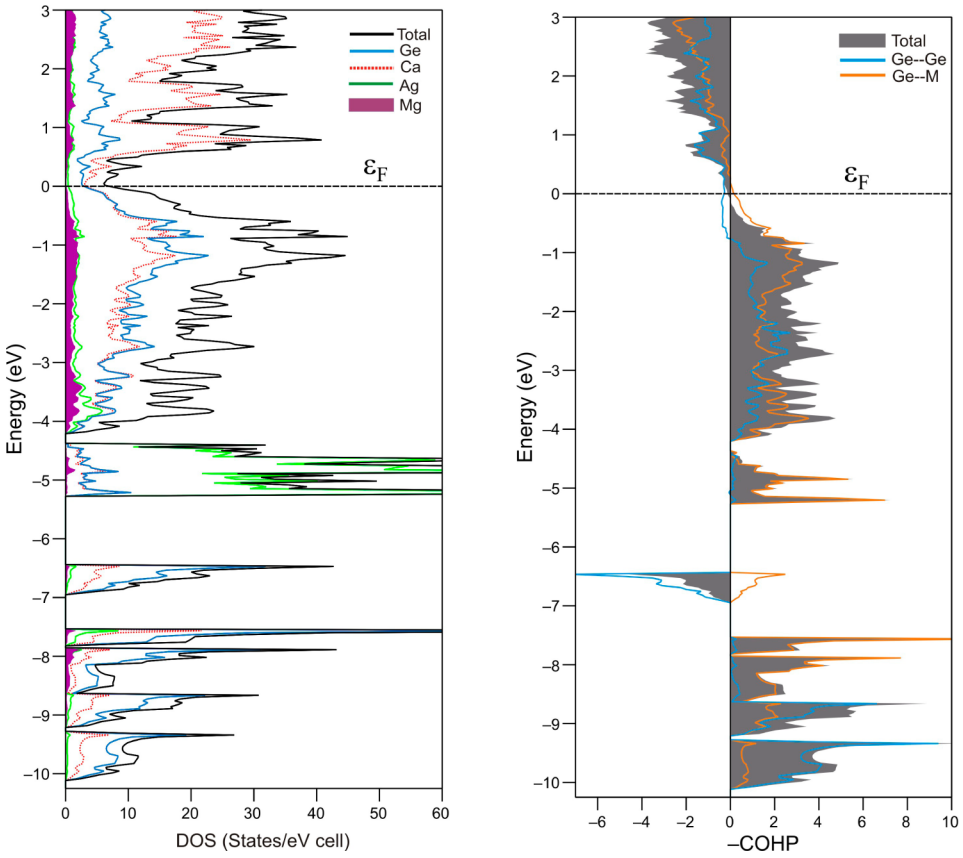

Figure 5. Density of states with atomic projections (left) and cumulative Ge−Ge and Ge−(Mg/Ag) crystal orbital Hamilton population (COHP) curves (right) for fully ordered model of $Ca_5MgAgGe_5$.

be determined by the electrostatic valency principle,[37] whereupon the sums of the strengths of the electrostatic bonds that reach each cation are somewhat adjusted to its charge. Hence, the divalent Mg^{2+} are surrounded by three Ge1 with formal charges of −4 and one Ge5 with a formal charge of −3, while the monovalent Ag^+ is surrounded by one Ge1 and three Ge2 with formal charges of −3 (Figure 2a). In other words, the Ge tetrahedra with the highest formal charge of −15 are centered by divalent Mg, and the monovalent Ag occupies the center of tetrahedra with a formal charge of −13. Because the amount of Ag in the Mg-dominated site almost equals the Mg occupancy in the mainly Ag site, the mixing seems to be incidental and the compound would ideally be ordered with a strict site preference between the two metals. We can speculate that, because of the electrostatic valency principle, two different valence states of the M metal are necessary to stabilize the structure and an eventual ternary variant should be expected only with mixed-valent metals. The electrostatic valency principle is a critical factor for the stability of ionic structures, but its effect is generally limited in intermetallic compounds because of the electron delocalization. Hence, the title compound **3** is a rare example of an intermetallic compound in which electrostatic forces are decisive for its structural stability. To verify the Mg/Ag site preference, total energy calculations for the title phase $Ca_5MgAgGe_5$ and the *anti*-structure $Ca_5AgMgGe_5$ (for which Mg and Ag positions are switched) were conducted in the generalized gradient approximation (GGA). The experimental lattice parameters are reproduced within less than 1%. The calculated total energy for the experimental model was 442 meV lower than the *anti*-structure. However, both models represent stable configurations, although the relatively modest energy difference may explain why the site preference is not strict.

Another puzzling issue, related to the electron deficiency, is to understand why a higher Mg content could not be obtained and ultimately why the Ag-free end-member "$Ca_5Mg_2Ge_5$" has remained elusive. A simple explanation may be the competitive formation of the thermodynamically more stable parent structure CaMgGe during synthesis at high temperature. This was usually observed in this structural family also with the rare-earth homologue.[29] A connected question is to explain the stability of the one-electron short phase $Ca_5Mg_{0.95}Ag_{1.05(1)}Ge_5$. The rare-earth members of this structural family are electron-rich according to the Zintl−Klemm rules. Also, the solid solution with Al of the $n = 4$ member, $Ca_3(Ag_{0.86}Al_{0.40})Ge_{2.74(1)}$, is again about 0.7 electrons rich according to the Zintl concept.[11] Moreover, the hypothetical ordered "Ca_3AgGe_3" ($n = 4$) will be one valence electron deficient per formula unit, but partial mixing with Ag will eventually result in a charge-balanced phase. Thus, these intergrowth systems may accommodate a slight electron excess, but apparently, electron deficiency is expected to induce higher instability and is, therefore, less tolerated.

Electronic Structure. To elucidate possible electronic factors and bonding characteristics that may account for the compound stability beyond the Zintl concept, first-principles band structure calculations were performed using the LMTO method. The calculated density of states (DOS) and projected DOS curves are given in Figure 5. It clearly shows a deep pseudogap at the Fermi level (E_F) that corresponds to 132

dx.doi.org/10.1021/ic500449d | *Inorg. Chem.* 2014, 53, 4724−4732

valence electrons per cell (or 43 ve/f.u), an indication that **3** is roughly electronically stabilized in contradiction with the Zintl concept that indicates a one-electron shortage. A real energy gap at the Fermi level is not expected because the binary parent structure CaGe is known to be metallic, although formally a Zintl phase.[46] However, a pseudogap was expected above E_F at 136 ve/cell (or 44 ve/f.u), as suggested by the Zintl concept. For the two-electron-deficient phases Ae_7Ge_6, a (pseudo)gap is always observed in the DOS plot above E_F at the Zintl limit of electron count. Therefore, the electronic structure of **3** provides an interesting case of conflicting views between the Zintl reasoning and the electronic structure in this class of materials. Other interesting features of the DOS are (i) the unusually strong Ca contribution to the states below the Fermi level, a feature that implies strong contribution to the covalent bonding of the system (the Ca contribution is nearly equal that of Ge from about −0.7 eV to E_F and becomes largely dominant above as expected); (ii) the highly localized states between −10 and −6 eV of the DOS curve that are mainly contributed by Ge-4*s* orbitals; and (iii) other highly localized states around −5 eV essentially contributed by Ag-5*d* orbitals, a result that is consistent with monovalent Ag^+. The valence band mainly involves Ge-4*p* and Ca-4*s*,3*d* orbitals. The overlapping of the empty Ca-3*d* orbitals with the valence band of the system is mainly responsible for the metallic characteristics of **3**.[47]

To investigate further the stabilizing factors of this phase, which is one electron short from the classical Zintl view, but virtually electron precise from its electronic structure perspective, a detailed analysis of the polar covalency within the polyanionic framework was conducted using COHP curves and their integration (−ICOHP values). The COHP curves of the combined Ge−Ge and M−Ge interactions in Figure 5 indicate that the polar−covalent bonding in the polyanionic framework is optimized on average. The Ge−Ge bonds are overall bonding, but with slight antibonding character just below the Fermi level starting at about −0.7 eV. The region of antibonding states nearly corresponds to the increase of Ca contribution to the DOS, meaning that these antibonding interactions may be compensated by Ca−Ge covalent bonding.[38] In contrast, the M−Ge bonds are roughly optimized. These antibonding Ge−Ge states correspond to partially filled π^* states, which is also observed in other phases with planar Ge chains, such as $LiCa_2Ge_3$ (Ge−Ge distances ranging from 2.46 to 2.61 Å).[48] The implication of the electron deficiency in **3** is that the antibonding π^* levels are significantly depopulated, which strengthens the Ge−Ge bonds within the Ge_4 tetramers. Complete depopulation of the π^* states is expected below E_F at about −0.7 eV, but this will result in significant depopulation of M−Ge and Ca−Ge bonding states. Therefore, the overall bonding in **3** is optimized by a combination of cation−anion coordinative bonds that compensate for the destabilizing effects of partially filling the Ge−Ge π^* states close to the Fermi level. As already pointed out earlier,[46] the four-membered Ge anions with zigzag chains and their planarity are intriguing because of the enhanced electrostatic repulsion between the lone pairs on Ge in negative valence states with no significant *s*−*p* orbital mixing. A possible stabilizing factor of the planar conformation will be a lower formal charge and π-bonding. However, in **3**, one electron deficiency per formula unit (f.u) is consistent with partially filled π-bonding levels. The −ICOHP values of selected bonds are listed in Table 4. Large −ICOHP values range from 2.36 to 2.51 eV/bond for the Ge−Ge contacts and are consistent with strong bonds. The Ca−Ge −ICOHP values up to 0.995 eV/bond, quite close to the lower value of 1.39 eV/bond for M1−Ge, also support strong Ca contributions to the overall polar−covalent bonding of the system. A more detailed analysis of individual Ge−Ge bonds in the tetramer indicated that only the terminal Ge2−Ge3 and Ge4−Ge5 π^* states are partially filled around E_F (Figure 6). As a general effect in intermetallic compounds, antibonding interactions at E_F are an effective way to relax the lattice potential gradient since it implies a delocalization of bonding electrons. Hence, the electronic structure of compound **3** confirms that the stability factors are far beyond the Zintl model and the active metal (Ca) cannot be considered as a mere valence electron donor. Unlike other electron-deficient phases, which is evident by their electronic band structures, the title phase $Ca_5MgAgGe_5$ with 132 ve/cell is truly stabilized electronically by Ca/M−Ge interactions and any increase of the electron count would result in an electron-rich phase, as indicated by the band structure calculations for the imaginary all-Mg phase "$Ca_5Mg_2Ge_5$" with 136 ve/cell (see the Supporting Information) and which is clearly one electron rich per formula unit with a pseudogap below E_F at 132 ve/cell. It is, therefore, likely that the asymmetry in the Ge_4 tetramer results in a strong gradient of the chemical potential between Ge atoms with the same formal charges that are not related by symmetry, and this is thwarted by violating the Zintl rules. Hence, achieving a closed-shell configuration for all atoms becomes secondary, as a gradient of chemical potential will have a more dramatic effect upon structural stability. Nature's solution is to create an electron deficiency coupled with Ge−Ge partial π^* antibonding interactions that is subsequently compensated by significant Ca contribution to the polar−covalent bonding of the system.

Table 4. Calculated −ICOHP Values for Selected Bonds in $Ca_5MgAgGe_5$

atom pair (× *n*)		distance/Å	−ICOHP (eV/bond) up to E_F
Ge1	−Mg2 (× 2)	2.745(1)	1.718
	−Ag1	2.752(1)	1.770
	−Mg2	2.857(1)	1.407
Ge2	−Ag1 (× 2)	2.711(1)	1.820
	−Ag1	2.846(1)	1.388
Ge2	−Ge3	2.557(1)	2.511
Ge3	−Ge4	2.569(1)	2.438
Ge4	−Ge5	2.581(1)	2.362
Ge5	−Mg2	2.799(1)	1.673
Ca	−Ge (× 17)	3.017−3.206(1)	0.995−0.576
Ca	$-Ge_{average}$	3.017−3.206(1)	0.747
Ca	−Ge2 (× 5)	3.017−3.206(1)	0.76
Ca	−Ge5 (× 7)	3.125−3.239(1)	0.84

CONCLUSION

The successful preparation and description of the missing member of the structural homology $R_{2+n}T_2X_{2+n}$, with $n = 3$, in a *hettotype* of the predicted structure, demonstrates further the difficulties to rationally prepare new intermetallic compounds with a predetermined structure and composition, even with the help of the intergrowth approach and the Zintl concept. The challenges are not only in the synthesis stage, where the difficulties to avoid competitive formation of more stable phases, in particular, have to be addressed, but also in assessing all the stability factors, such as electronic, geometrical, and even

dx.doi.org/10.1021/ic500449d | Inorg. Chem. 2014, 53, 4724−4732

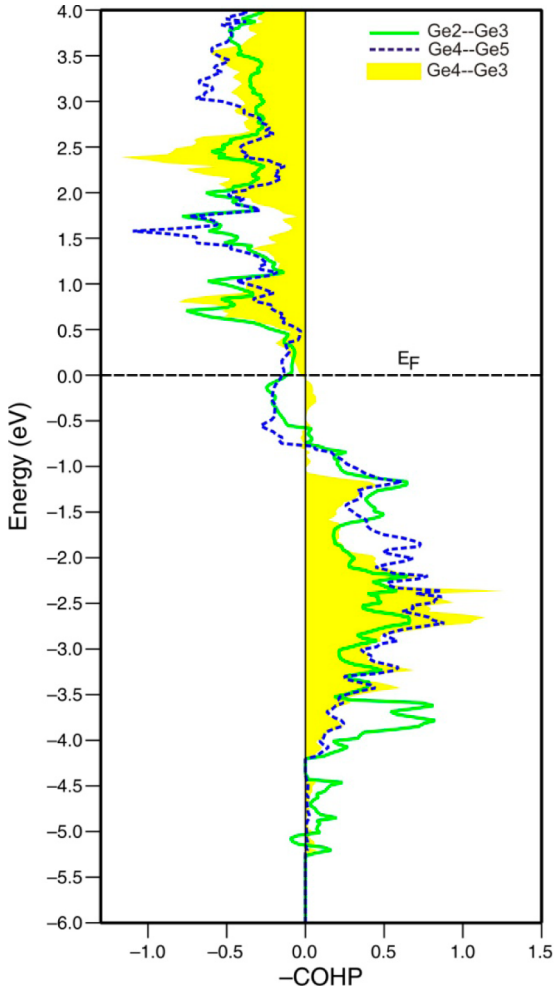

Figure 6. Crystal orbital Hamilton population (COHP) curves for the three Ge−Ge interactions in the Ge_4 tetramer for $Ca_5MgAgGe_5$. The corresponding interactions are depicted in Figure 4.

intrinsic chemical properties of the elements involved, since all of these have decisive impacts on the structure stability. Compound **3** represents a remarkable example of true electronic stabilization by factors beyond the Zintl−Klemm concept, as the bonding optimization is achieved by a combination of homonuclear localized bonds and "cation−anion" interactions. Furthermore, the unexpected Mg/Ag site preference can be explained by the electrostatic valency principle, indicating that ionic interactions are also decisive for the structure stability, and this is supported by the VASP total energy calculations. It is most likely that the asymmetry in the Ge_4 tetramer results in a strong gradient of chemical potential within the Ge_4 tetramers, a feature that is apparently corrected by violating the 8−*N* rule. Our ongoing investigations of some isostructural structures with paramagnetic transition metals $Ca_5M_{1-x}Ag_{1+x}Ge_5$ (M = Mn, Co), in which larger electron deficiency is observed, seem to indicate a possible stabilization by unusual magnetic exchange interactions.

■ ASSOCIATED CONTENT

Supporting Information

Detailed crystallographic data in CIF format, comparison between the predicted model and the final model, projected DOS for Ca (*s*- and *d*-orbitals) and Ge (*s*- and *p*-orbitals) for $Ca_5MgAgGe_5$ (132 ve/cell), as well as total and projected DOS for the hypothetical "$Ca_5Mg_2Ge_5$" (136 ve/cell). This material is available free of charge via the Internet at http://pubs.acs.org.

■ AUTHOR INFORMATION

Corresponding Authors

*E-mail: simeon.ponou@chem.lu.se (S.P.).
*E-mail: gmiller@iastate.edu (G.J.M.).

Notes

The authors declare no competing financial interest.

■ ACKNOWLEDGMENTS

This work was financially supported by the Swedish National Science Council (VR). The authors also thank the National Science Foundation (NSF DMR 10-05765 and 12-09135) for generous financial support.

■ REFERENCES

(1) (a) Andersson, S. *Angew. Chem.* **1983**, *95*, 67−79;(b) *Angew. Chem., Int. Ed. Engl.* **1983**, *22*, 69−81.
(2) Parthe, E.; Chabot, B. A.; Cenzual, K. *Chimia.* **1985**, *39*, 164−174.
(3) Zürcher, F.; Wengert, S.; Nesper, R. *Inorg. Chem.* **1999**, *38*, 4567−4569.
(4) Guo, S.-P.; You, T.-S.; Jung, Ya-Ho; Bobev, S. *Inorg. Chem.* **2012**, *51*, 6821−6829.
(5) Zhao, J. T.; Parthé, E. *Acta Crystallogr.* **1989**, *C45*, 1853−1856.
(6) Yarmolyuk, Y. P.; Grin, Y.; Gladyshevskii, E. I. *Sov. Phys. Crystallogr.* **1977**, *22*, 416−419.
(7) Gladyshevskii, E. I.; Kotur, B. Y. *Sov. Phys. Crystallogr.* **1978**, *23*, 533−535.
(8) Gladyshevskii, E. I.; Kotur, B. Y. *Sov. Phys. Crystallogr.* **1983**, *28*, 271−273.
(9) Pavlyuk, V. V.; Bodak, O. I. *Inorg. Mater.* **1992**, *28*, 877−879.
(10) Siggelkow, L.; Hlukhyy, V.; Fässler, T. F. *Eur. J. Inorg. Chem.* **2012**, 987−997.
(11) Ponou, S.; Lidin, S. *Z. Anorg. Allg. Chem.* **2013**, *639*, 35−40.
(12) Ponou, S.; Lidin, S. *Z. Anorg. Allg. Chem.* **2009**, *635*, 2143−2146.
(13) Banenzoué, C.; Ponou, S.; Lambi, J. N. *Acta Crystallogr.* **2009**, *E65*, i90.
(14) Kauzlarich, S. M., Ed. *Chemistry, Structure, and Bonding of Zintl Phases and Ions*; VCH: New York, 1996.
(15) *CrysAlis CCD and CrysAlis RED*; Oxford Diffraction Ltd.: Abingdon, U.K., 2006; p171.31.2.
(16) Sheldrick, G. M. *Acta Crystallogr.* **2008**, *A64*, 112−122.
(17) *SHELXTL*, version 5.1; Bruker AXS Inc.: Madison, WI, 1998.
(18) Brandenburg, K.; Putz, H. *DIAMOND*; Crystal Impact GbR: Bonn, Germany, 1999.
(19) von Barth, U.; Hedin, L. *J. Phys. C: Solid State Phys.* **1972**, *5*, 1629−1642.
(20) Krier, G.; Jepsen, O.; Burkhardt, A.; Andersen, O. K. *TB-LMTO-ASA Program*, version 4.7; Max Planck Institute for Solid-State Research: Stuttgart, Germany, 2000.
(21) Jepsen, O.; Anderson, O. K. *Z. Phys. B* **1995**, *97*, 35.
(22) Dronskowski, R.; Blöchl, P. E. *J. Phys. Chem.* **1993**, *97*, 8617.
(23) Blöchl, P. E. *Phys. Rev. B* **1994**, *50*, 17953−17979.
(24) (a) Kresse, G.; Hafner, J. *Phys. Rev. B* **1993**, *47*, 558−561. (b) Kresse, G.; Furthmüller, F. *Comput. Mater. Sci.* **1996**, *6*, 15−50;(c) *Phys. Rev. B* **1996**, *54*, 11169−11186. (d) Kresse, G.; Joubert, D. *Phys. Rev. B* **1999**, *59*, 1758−1775.
(25) Perdew, J. P.; Burke, K.; Ernzerhof, M. *Phys. Rev. Lett.* **1996**, *77*, 3865−3868.
(26) Villars, P., Calvert, L. D., Eds. *Pearson's Handbook of Crystallographic Data for Intermetallic Phases*, 2nd ed.; American Society for Metals: Materials Park, OH, 1998.
(27) Parthé, E.; Chabot, B. In *Handbook on the Physics and Chemistry of Rare Earths*; Gschneidner, K. A., Eyring, L., Eds.; Elsevier: Amsterdam, 1985; pp 113−334.

(28) Ponou, S. *Eur. J. Inorg. Chem.* **1998**, 4139−4147.
(29) Merlo, F.; Fornasini, M. L.; Pani, M. *J. Alloys Compd.* **2005**, *387*, 165−171.
(30) Eckerlin, P.; Meyer, H. J.; Wölfel, E. R. *Z. Anorg. Allg. Chem.* **1955**, *281*, 322−328.
(31) Bärnighausen, H. *Commun. Math. Chem.* **1980**, *9*, 139−175.
(32) Müller, U. *Z. Anorg. Allg. Chem.* **2004**, *630*, 1519−1537.
(33) Kersting, M.; Johnscher, M.; Pöttgen, R. *Z. Kristallogr.* **2013**, *228*, 635−642.
(34) Fickenscher, Th.; Pöttgen, R. *J. Solid State. Chem.* **2001**, *161*, 67−72.
(35) Landrum, G. A.; Hoffmann, R.; Evers, J.; Boysen, H. *Inorg. Chem.* **1998**, *37*, 5754−5763.
(36) Nuspl, G.; Polborn, K.; Evers, J.; Landrum, G. A.; Hoffmann, R. *Inorg. Chem.* **1996**, *35*, 6922−6932.
(37) Pauling, L. *The Nature of the Chemical Bond*, 2nd ed.; Cornell University Press: Ithaca, NY, 1945.
(38) Ponou, S.; Fässler, T. F.; Tobias, G.; Canadell, E.; Cho, A.; Sevov, S. C. *Chem.—Eur. J.* **2004**, *10*, 3615−3621.
(39) Alemany, P.; Alvarez, S.; Hoffmann, R. *Inorg. Chem.* **1990**, *29*, 3070−3073.
(40) Alemany, P.; Llunell, M.; Canadell, E. *Inorg. Chem.* **2006**, *45*, 7235−7241.
(41) Siggelkow, L.; Hlukhyy, V.; Fässler, T. F. *J. Solid State. Chem.* **2012**, *191*, 76−89.
(42) You, T.-S.; Jung, Y.; Bobev, S. *Dalton Trans.* **2012**, *41*, 12446−12451.
(43) Sun, Z.-M.; Xia, S.-Q.; Huang, Y.-Z.; Wu, L.-M.; Mao, J.-G. *Inorg. Chem.* **2005**, *44*, 9242−9246.
(44) Miller, G. J. *Eur. J. Inorg. Chem.* **1998**, 523.
(45) You, T.-S.; Han, M.-K.; Miller, G. J. *Inorg. Chim. Acta* **2008**, *361*, 3053−3062.
(46) Reyes, E. C.; Stalder, E. D.; Mensing, C.; Budnyk, S.; Nesper, R. *J. Phys. Chem. C* **2011**, *115*, 1090−1095.
(47) Mudring, A. V.; Corbett, J. D. *J. Am. Chem. Soc.* **2004**, *126*, 5277−5281.
(48) Müller, W.; Schäfer, H.; Weiss, A. *Z. Naturforsch. B* **1971**, *26*, 5−7.